ROYAL SOCIETY OF CHEMISTRY

PAPER

Check for updates

Atmospheric brown carbon from biofuel pyrolysis: comparative analysis of dung and wood sources

Diego Calderon-Arrieta, [ID] [a] Jessica Knull,[a] Shudeepta Sarker,[a] JingKai Wang,[a] Larissa Evans,[a] Julius Ese,[a] Seth M. Koloski,[a] Abigail M. Smith,[a] Nyiri Hajian,[a] Kirby Hill,[a] Baerbel Sinha [ID] [c] and Alexander Laskin [ID] *[ab]

Brown carbon (BrC), a class of light-absorbing organic compounds produced during biomass burning, plays an important role in atmospheric radiative transfer and air quality. However, accurate representation of BrC in atmospheric models remains limited by insufficient understanding of its complex molecular composition and variable optical properties. In this study, we present a comparative molecular-level characterization of BrC chromophores in laboratory-generated organic aerosol (OA) mixtures representing pyrolysis components of wood-burning (WBOA) and dung-burning (DBOA) emissions, corresponding to two commonly used categories of residential biomass fuels. Using a hyphenated high-performance liquid chromatography-photodiode array-high-resolution mass spectrometry (HPLC-PDA-HRMS) platform, we analyzed these mixtures alongside 100 BrC reference compounds and evaluated the composition, volatility, and light-absorbing properties of their constituent species. WBOA was found to be enriched in CHO-class chromophores primarily derived from lignin decomposition, while DBOA contained a higher abundance of CHON and CHN classes corresponding to reduced N-containing organic compounds (RNOCs). N-heterocyclic compound classes, such as pyrrole- and pyrazine-containing species, were plausibly detected in the DBOA mixture. Double bond equivalency analysis identified a substantial fraction of potential BrC chromophores in both mixtures, although their chemical classes, structural features, and optical properties differed significantly. Volatility basis set modeling revealed that WBOA components are less volatile and remain in the particle phase under a wider range of atmospheric conditions, while DBOA constituents partition more readily to the gas phase. These findings underscore the need for more detailed treatment of BrC variability in chemical transport models, especially in regions where dung is a dominant household fuel. This study advances molecular-level understanding of BrC and highlights the importance of fuel type in shaping its atmospheric behavior.

Environmental significance

This study shows how compositional differences between dung- and wood-derived biofuels shape the atmospheric behavior of biomass burning emissions, with implications for atmospheric chemistry, radiative forcing, and air quality. It shows that the molecular composition and volatility of emitted organic compounds vary significantly by fuel type, influencing their gas-particle partitioning, atmospheric lifetime, and light-absorbing characteristics. Emissions from dung burning are enriched in nitrogen-containing, volatile species, while wood burning produces more low-volatility, lignin-derived compounds that persist in the particle phase. These findings underscore the need for fuel-specific emission inventories and volatility-resolved parameterizations in atmospheric models—particularly in regions where residential biomass burning remains a dominant energy source.

1 Introduction

Atmospheric light-absorbing organic compounds, known as brown carbon (BrC), are common constituents of biomass burning organic aerosol (BBOA) emitted from wildfires, prescribed forest management burns, agricultural burning, and the use of biomass fuels for household heating and cooking.[1–7] BBOA and its BrC components play significant roles in atmospheric chemistry, environmental processes, and public health.[1–3,5–9] However, the complex and variable molecular composition of BBOA introduces substantial uncertainties into models that aim to predict its effects on radiative forcing and air quality.[7,10–13] This challenge is becoming increasingly critical, as both wildfire activity and biomass fuel use are expected to rise, amplifying the atmospheric burden and global impacts of BBOA.[11,14–18] Improving BBOA representation in atmospheric

[a]Department of Chemistry, Purdue University, West Lafayette, IN 47907, USA. E-mail: alaskin@purdue.edu

[b]Department of Earth, Atmospheric, and Planetary Sciences, Purdue University, West Lafayette, IN 47907, USA

[c]Department of Earth and Environmental Sciences, Indian Institute of Science Education and Research Mohali, Sector 81, SAS Nagar, Manauli PO, Punjab, 140306, India

© 2026 The Author(s). Published by the Royal Society of Chemistry

Environ. Sci.: Atmos., 2026, 6, 61–75 | 61

models[7,19,20] requires a thorough understanding of its molecular composition and optical properties, which are shaped by various factors such as burning conditions,[5,21,22] fuel type,[4,14,21,23–25] and atmospheric aging.[3–5,26,27] To address these complexities, recent studies have focused on field-based measurements,[28–30] experiments with laboratory-generated BBOA proxies,[14,25,31,32] and the applications of machine learning techniques.[33,34] Additionally, geographic source profiling of BBOA has also advanced as a means of capturing BrC spatial variability and regional contributions to radiative forcing of climate.[7,12,25,35,36] Despite these efforts, current characterization of BrC optical and chemical properties remains incomplete, limiting its adequate representation in atmospheric models and constraining its radiative effects.

Residential BBOA emissions are emerging as a significant source of BrC in developing countries with rapidly growing populations.[7,37–39] In regions where wood biomass is scarce, animal waste (such as cow and yak dung) is commonly used as inexpensive biofuel to meet household energy needs.[11,15,40,41] The chemical composition of wood biomass differs substantially from that of animal waste, leading to the emissions of wood-burning and dung-burning organic aerosols (WBOA and DBOA, hereafter) with distinct molecular signatures and BrC characteristics.[14,24,39,42] Studies have shown that WBOA is typically enriched in CH and CHO species,[14,39,42] whereas DBOA contains a higher proportion of nitrogen-containing CHON compounds.[11,14] Despite these compositional differences, atmospheric models often generalize BBOA properties based on emissions from wood-derived biofuels, often overlooking the variability introduced by dung biofuels.[11,43] Characterizing the emission components from WBOA and DBOA sources can streamline efforts to quantify and represent the chemical diversity of BBOA in atmospheric studies. Here, we conducted a molecular-level analysis of laboratory-generated pyrolysis proxy mixtures of WBOA and DBOA and compared the results to a recently published reference list of individual BrC chromophores.[25] Comprehensive chemical characterization was performed using a hyphenated analytical platform combining high-performance liquid chromatography, photodiode array detection, and high-resolution mass spectrometry (HPLC-PDA-HRMS), complemented by organic carbon quantification. The results show that the WBOA mixture contains a substantial fraction of previously identified BrC chromophores. In contrast, the DBOA mixture is dominated by relatively reduced nitrogen-containing organic compounds (RNOCs) that are yet underrepresented in existing BrC reference inventories, underscoring the need to expand molecular characterization efforts to include BBOA emissions from animal-waste-derived-biofuels.

2 Materials and methods

2.1 Generation of proxy mixtures and total organic carbon (TOC) assessment

Dry cow dung cakes, prepared for household use as solid biofuel, were collected from the storage pile of cow dung users in villages located in Himachal, India in 2019 and stored in airtight Ziplock bags at room temperature. They were transported to the US in an airtight plastic container at room temperature as well. Fig. S1 shows a representative photo of the dung cake materials stored in the plastic container. To generate the DBOA proxy mixture, ~100 g of crushed dung sample was heated at ~535 °C in a N_2-purged dry distillation apparatus equipped with a room-temperature water condenser (previously described in our studies).[31,44] Fume emissions were collected with acetonitrile (ACN, Fisher Scientific, Optima LC-MS grade) and gently-evaporated in a TurboVap LV system (Biotage, 416200) to obtain the DBOA analytes, which were stored at −4 °C between analyses. A schematic of the distillation setup used for generating the DBOA mixture is shown in Fig. S1 (SI note A). The WBOA proxy mixture used in this study was prepared following the same procedure described in our previous work, where it was referred to as PO_1.[31,44] The organic carbon (OC) content of the WBOA and DBOA mixtures was quantified using aqueous solutions aspirated through a total organic carbon (TOC) analyzer (Sievers, M9 Portable).[45] TOC content ($\mu g\ mL^{-1}$) for each mixture was obtained based on the difference between organic-derived dissolved carbon dioxide (CO_2) and inorganic-derived CO_2 in the instrument's linear response range, thereby determining measured OC-to-total mass ratios (m_{OC}/m_{total}) that would ascertain OC mass sampled by the HPLC instrument. A more detailed description of the TOC operational settings is provided in SI note B, and calibration plots used to verify the instrument's linear response range are shown in Fig. S2, yielding m_{OC}/m_{total} ratios of 0.29 and 0.26 for DBOA and WBOA, respectively.

2.2 HPLC-PDA-HRMS analysis

A pre-filtered 1000 $\mu g\ mL^{-1}$ solution of DBOA dissolved in ACN was analyzed using a Vanquish HPLC system equipped with a PDA detector and coupled to a high-resolution Orbitrap mass spectrometer (all from ThermoFisher scientific). A solvent blank was also analyzed to account for chemical and optical interferents originating from the solvent and mobile phase. Dual 10 μL injections were performed in triplicate to ensure reproducibility of PDA measurements and comprehensive molecular characterization. The analysis employed both electrospray ionization (ESI) and dopant-assisted atmospheric pressure photoionization (APPI) sources, with data acquired in alternating positive and negative ion modes.[31,46–48] Chromatographic separation was achieved on a reversed-phase Luna C18 column (Phenomenex, 00F-4252-B0) protected with a SecurityGuard C18 guard cartridge (Phenomenex, AJ0-4286), both maintained at 25 °C, using a previously-established gradient elution protocol.[31,44] An explicit summary outlining the HPLC-PDA-HRMS operational settings is provided in SI note C. The WBOA sample was analyzed using identical instrumental conditions, as detailed in our previous studies,[31,44] providing a consistent basis for comparison with the DBOA results presented here.

2.3 Calculation of $MAC_{OC}(\lambda)$ and AAE from PDA records

Wavelength-dependent mass absorption coefficient ($MAC_{OC}(\lambda)$, $m^2\ g^{-1}$) values of DBOA and WBOA samples were obtained from HPLC-PDA records using the equation displayed below.[49]

$$\text{MAC}_{\text{OC}}(\lambda)\left[\text{m}^2\text{g}^{-1}\right]$$

$$= \frac{\text{Abs}(\lambda)[\mu\text{AU}] \times \Delta t[\text{min}] \times \ln(10) \times F\left[\text{mL min}^{-1}\right]}{b[\text{cm}] \times 10 \times m_{\text{inj}}[\text{ng}]} \quad (1)$$

where, $\text{Abs}(\lambda)$ corresponds to the absorbance measured at wavelength λ integrated over the entire elution time, Δt represents the chromatographic separation time frame (0−100 min), F reflects the HPLC flow rate (0.2 mL min^{-1}), b is the path length in the LightPipe flow cell (1.0 cm), and m_{inj} represents the injected OC mass of the samples. Combined conversion of μAU to AU, cm^3 to m^3, cm to m, and ng to g units yields a 10^{-1} coefficient. Based on the calibrated $m_{\text{OC}}/m_{\text{total}}$ ratios (Fig. S2), the injected OC mass was estimated to be 2900 ng for DBOA and 2500 ng for WBOA. These values define the m_{inj} term in eqn (1), yielding OC-normalized $\text{MAC}_{\text{OC}}(\lambda)$ values.

To relate the absorbance contributions of constituent molecules to their polarity and aromaticity, three broad retention time fractions were defined based on our previous work: Fraction A (3−40 min; monoaromatics), Fraction B (40−65 min; lignin fragments), Fraction C (65−100 min; substituted polycyclic aromatic hydrocarbons, PAHs).[44] Contributions of each fraction to the total $\text{MAC}_{\text{OC}}(\lambda)$ were quantified using eqn (2).

$$\text{MAC}_{\text{OC}}(\lambda)_i\left[\text{m}^2\text{g}^{-1}\right] = \text{MAC}_{\text{OC}}(\lambda)\left[\text{m}^2\text{g}^{-1}\right]$$
$$\times \left(\frac{\text{Abs}(\lambda)_i[\mu\text{AU}] \times \Delta t[\text{min}]}{\text{Abs}(\lambda)[\mu\text{AU}] \times \Delta t[\text{min}]}\right) \quad (2)$$

where, $\text{MAC}_{\text{OC}}(\lambda)_i$ corresponds to the integrated UV-vis absorbance of the specific segment i and Δt_i denotes its elution time range. The absorbance contributions from well-resolved major chromophores were calculated using this approach. Wavelength-dependent light absorption was characterized by calculating absorption Ångström exponent (AAE) values over 280–405 nm and 300–405 nm, derived from slopes of log–log linear regressions of $\text{MAC}_{\text{OC}}(\lambda)$ versus wavelength. Triplicate PDA measurements provided mean and standard deviation for both the AAE and log10($\text{MAC}_{\text{OC\_405 nm}}$). The resulting AAE slope factors for the WBOA and DBOA samples are shown in Fig. S3 (SI note D).

2.4 BrC reference compound comparison and data analysis

Four BrC reference solutions (G1–G4, each containing 25 BrC compounds)[25] were analyzed under the same HPLC-PDA-HRMS conditions described above. Compounds in G2–G4 were dissolved in methanol, while the G1 solution was originally prepared in ACN/dichloromethane/hexane (2 : 1 : 1, v/v).[46] To ensure consistency across all solutions, the G1 residues were reconstituted in methanol after the solution was evaporated using the previously-mentioned TurboVap LV system. All solutions were diluted to 10 μg mL^{-1} prior to analysis. Retention times and UV-vis absorbance spectra of reference compounds were compared to those observed in the DBOA and WBOA samples to assess overlap. Data were processed in MZMine 2.53, an open-source LC-MS data processing software (https://github.com/mzmine).[50] Detailed procedures for generating extracted ion chromatograms (EICs) are described in SI note E. Ion species considered in ESI($\pm$) modes included [M + H]$^+$,

[M + Na]$^+$, and [M–H]$^-$, while in APPI($\pm$) modes included [M + H]$^+$, [M]$^{\cdot+}$, [M–H]$^-$, and [M]$^{\cdot-}$. Elemental formulas were assigned using custom-built Excel macros and the MIDAS molecular formula calculator (v. 1.2.3; National High Magnetic Field Laboratory, USA), based on higher-order Kendrick mass defect analysis.[51] Assignments were constrained to $C_\infty H_\infty O_{0-10} N_{0-3} Na_{0-1}$, with a mass tolerance of ±3.0 ppm. Assigned compounds were categorized into CH, CHO, CHON, or CHN classes. Overall, more than 82% of detected HRMS features were successfully assigned (Fig. S4, SI note E). Among all ionization modes, ESI(+) was most effective for the DBOA mixture, detecting a broader range of constituents than APPI(+), as illustrated in Fig. S5 (SI note E). An UpSet diagram in Fig. S6 summarizes the overlap and exclusivity of masses detected in ESI(+), APPI(+), or both modes. Fifteen DBOA features (#71−85) and twenty-three previously identified WBOA features [as labeled in Hettiyadura et al. (2021)][31] were chemically characterized by correlating PDA and HRMS data. Prominent chromophores detected by HPLC-PDA in both samples are shown in Fig. S7 (SI note F), with detailed EICs of major DBOA features presented in Fig. S8 (SI note F). Key WBOA chromophores from Fractions A and B are displayed in Fig. S9 and S10 (SI note F), respectively. Comprehensive listings of UV-vis absorbance spectra, observed m/z values, elemental formulas, reference compound identities, and plausible molecular structures for major DBOA and WBOA chromophores are provided in Tables S1 and S2 (SI note F).

To assess molecular characteristics of the identified constituents in the DBOA and WBOA mixtures, visualizations were generated using common molecular metrics, including double bond equivalency (DBE) plots and van Krevelen (VK) diagrams.[52,53] DBE offers insight into the degree of unsaturation within organic compounds and helps infer the presence of potential BrC chromophores.[32,44,46] DBE values were calculated using the following equation:[53]

$$\text{DBE} = C - \frac{H}{2} + \frac{N}{2} + 1 \quad (3)$$

where, C, H, and N denote the number of carbon, hydrogen, and nitrogen atoms in the elemental formula of each compound. Comprehensive DBE distributions for all four ionization modes are presented in Fig. S11 (SI note G). APPI(+) HRMS spectra and their associated DBE plots are shown in Fig. S12. These plots help identify potential nonpolar BrC chromophores in both mixtures. Additionally, VK diagrams[52] were used to evaluate the polarity and functional group composition of the molecular constituents. These diagrams for the DBOA and WBOA samples are shown in Fig. S13 (SI note G).

2.5 Assessment of component volatility in DBOA and WBOA mixtures

Gas-particle partitioning behavior of components in the DBOA and WBOA mixtures was evaluated by constructing volatility basis set (VBS) distributions.[54,55] Detailed procedures are provided in SI note H. Briefly, molar fractions of identified components were approximated based on the integrated peak areas of their EICs. Volatility of each compound, expressed as

the gas-phase saturation mass concentrations (C_T^*, µg m^{-3}) as a function of temperature (T, K), was estimated through a multi-step calculation approach. First, reference saturation concentrations at 298 K (C_{298K}^*, µg m^{-3}) were estimated using the semi-empirical 'molecular corridor' (MC) parameterization.[56] These initial values were then refined to obtain more accurate saturation concentrations C_{298K}^* by applying a trendline correction derived from the deviation between MC-predicted and experimentally measured volatilities of dominant WBOA constituents (referred to as PO$_1$ in our previous publication).[57,58] Next, compound-specific enthalpies of vaporization (ΔH_{vap}^*, kJ mol^{-1}) were estimated using a semi-empirical relationship $\Delta H_{vap} = -11 \times \log C_{298K}^* + 85$.[59] This expression has been shown to perform well for major components of WBOA and for field-collected anthropogenic aerosols significantly influenced by BBOA emissions.[60] Finally, temperature-dependent saturation concentrations (C_T^*), were calculated using the Clausius–Clapeyron equation (eqn (4)), incorporating the component-specific input values of C_{298K}^* and ΔH_{vap}^*.

$$C_T^*\left[\frac{\mu g}{m^3}\right] = C_{298K}^*\left[\frac{\mu g}{m^3}\right]\left(\frac{298K}{T[K]}\right)\exp\left(-\frac{\Delta H_{vap}^*}{R[kJ\ mol^{-1}K^{-1}]}\right)$$
$$\left(\frac{1}{T[K]} - \frac{1}{298K}\right) \quad (4)$$

Using the calculated C_T^* values and estimated molar fractions of individual components, gas-particle partitioning behavior of DBOA and WBOA components was evaluated using VBS distributions[54,55] constructed separately for each mixture. The VBS distributions were constructed across broad ranges of total organic mass concentrations (tOM, 1–1000 µg m^{-3}) and temperatures (T, 273−323 K), enabling assessment of the partitioning dynamics under variable atmospheric conditions. The resulting VBS plots illustrating dilution-driven gas-particle partitioning for both mixtures are presented in Fig. S14, while Fig. S15 illustrates corresponding shifts due to atmospheric cooling (SI note H). Additionally, gas-particle partitioning behavior was evaluated using an alternative semi-empirical parameterization developed to estimate upper-limit partitioning trends.[61] VBS distributions based on this second approach are summarized in Fig. S16.

3 Results and discussion

3.1 Characterization of major DBOA chromophores

Fig. 1 presents the characterization of major chromophoric species and their absorbance contributions in the DBOA mixture. The HPLC-PDA chromatogram is segmented into three polarity-based retention time windows: monoaromatics (Fraction A, 3–40 min), lignin fragments (Fraction B, 40–65 min), and substituted polyaromatics (Fraction C, 65–100 min), following the framework established in our previous work.[44] Panels (a) and (b) display fifteen labeled PDA features alongside their EICs. The corresponding chromophores (#71–85) identified in the DBOA sample are distinct from those previously reported for the WBOA (or PO$_1$) mixture (#1–62) by Hettiyadura *et al.*

(2021).[31] Plausible structural assignments for these DBOA chromophores are supported by their elemental formulas, UV-vis absorbance spectra, and literature references, as summarized in Table S1 (SI note F). Chromophores are color-coded by molecular class: CHO (blue), CHN (green), or CHON (orange). Most identified DBOA chromophores elute within Fraction A and include substituted furans (#73, $C_6H_8O_2$), phenolic compounds (#74, $C_6H_6O_3$; #84, $C_{10}H_{12}O$), and RNOCs such as pyrazines (#78, $C_8H_{12}ON_2$; #82, $C_{15}H_{18}ON_2$). This dominance of these early-eluting, lower-molecular-weight species reflects the compositional characteristics of dung-based biofuels. Cattle primarily consume lignin-deficient feedstocks such as wheat, rice straw, and maize straw,[24,62] which yield fewer lignin-derived and PAH compounds upon dung pyrolysis. As a result, later-eluting species commonly associated with lignin breakdown (Fraction B) and PAHs (Fraction C) – which are prominent in WBOA mixtures[25,31,32] – are absent from the DBOA sample.

The DBOA mixture exhibits a notable lack of detectable BrC reference compounds from G1–G4 mixtures. Although PDA feature #79 coelutes with vanillin based on retention time, its UV-vis absorbance spectrum does not match the known spectrum of vanillin (Table S1, SI note F), suggesting that vanillin, if present, exists at trace levels and is obscured by a coeluting stronger chromophore. While the G1–G4 reference mixtures include N-containing compounds such as 4-nitrocatechol ($C_5H_6O_4N$), a recognized tracer for biomass burning,[63,64] the majority of CHON reference species are nitroaromatics typically formed through atmospheric photooxidation in the presence of nitrogen oxides (NO$_x$).[65,66] In contrast, the N-containing species identified in the DBOA sample are mostly RNOCs, including various heterocyclic compounds that are readily detected in ESI(+) mode.[67,68] These results highlight the chemically reduced nature of N-containing BrC chromophores in DBOA compared to the oxidized nitroaromatic species commonly associated with aged WBOA emissions.

It is important to note that the RNOCs identified in this study are pyrolysis products formed under anoxic conditions, reflecting thermal degradation pathways distinct from those occurring in typical household cookstove emissions reported in earlier literature.[69–72] Nevertheless, characterizing these pyrolysis-derived RNOCs is essential for expanding our understanding of biomass burning emissions, as oxygen-limited smoldering is common in many real-world contexts, including residential cookstoves, agricultural burning, prescribed burns, and naturally-occurring wildfires.[73] These conditions generate chemically distinct RNOCs that are often missing from current emission inventories, yet may significantly impact atmospheric reactivity, radiative properties, and toxicological outcomes.[15,36,37] They also offer valuable chemical insights for improving the source attribution of biomass burning emissions. For example, the DBOA chromophores identified in this pyrolysis study (anoxic conditions), exhibit lower oxygenation levels and fewer acidic moieties such as carboxylic acids, compared to ambient samples from Indian cow dung-fueled cookstoves,[70] that involve dung burning in an oxygen-containing atmosphere. Compounds like ferulic acid, benzoic acid, and vanillic acid – detected in those ambient studies but
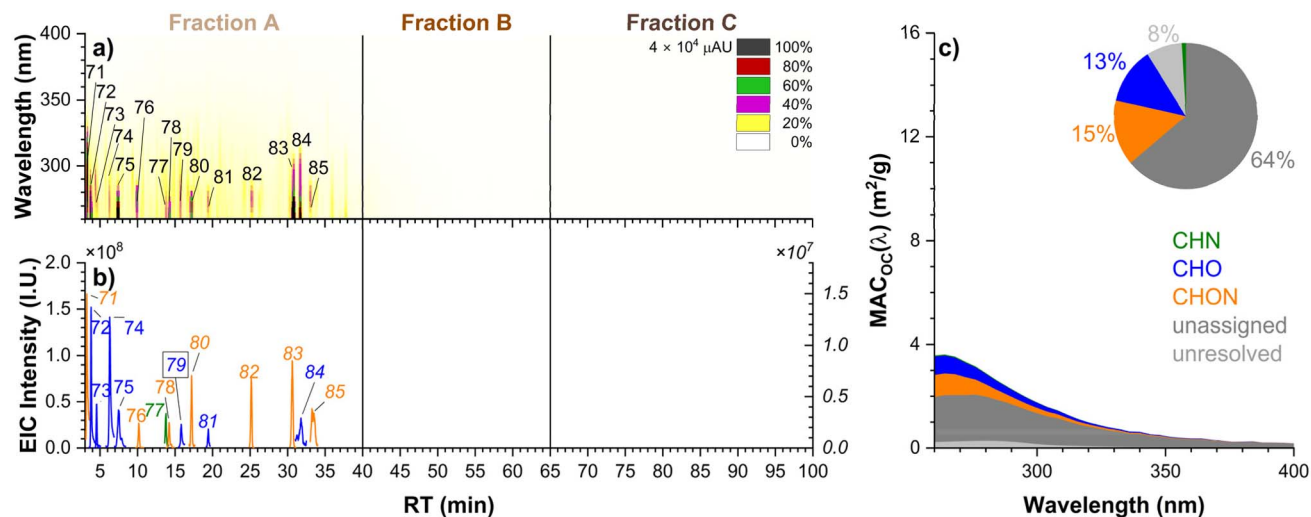
Fig. 1 Characterization of major chromophoric compounds in the DBOA sample. (a) HPLC‑PDA absorbance heatmap chromatogram, (b) HPLC‑HRMS extracted ion chromatogram overlay, (c) fractional $MAC_{OC}(\lambda)$ contributions of major DBOA chromophores. Assigned PDA features are numbered in order of retention time and color‑coded based on compound class. Italicized labels indicate MS features with intensities referenced to the right-hand axis; boxed labels denote BrC chromophores matched to compounds in the G1–G4 reference mixtures. Among the identified chromophores, CHON and CHN compounds contribute 16% of the total absorbance, followed by 13% contributed by CHO species.

not in our pyrolysis experiments – are likely formed under oxidative burning conditions. Conversely, the furan derivatives detected in the anoxic dung-based pyrolysis products are absent in the source-sampled aerosol[70] but present in dung burning smoke with relatively high gas-phase emission factors (0.1 to 0.5 g kg^{-1} of fuel),[69] indicating that the heat above the stove may have partitioned these compounds into the gas phase due to their high volatility.[74] Notably, Stewart *et al.* (2021)[71,72] successfully detected substituted furans and other highly volatile components from cookstove emissions, likely due to the cooling of the flue gas before sampling. Developing this robust portfolio of pyrolysis-based DBOA compounds will strengthen emission inventories and enhance molecular-level source apportionment, particularly in regions like Southeast Asia where such emissions remain under-characterized.

Panel (c) of Fig. 1 illustrates the relative contributions of identified chromophores to the total light absorption, expressed as fractions of the $MAC_{OC}(\lambda)$ for the DBOA mixture. Collectively, the assigned CHN, CHO, and CHON chromophores account for over 25% of total absorbance, with N-containing species contributing more significantly than CHO compounds. An additional ~8% is attributed to unresolved, highly polar chromophores, likely resulting from limited chromatographic resolution under the current stationary phase and flow rate conditions. Notably, 64% of the total absorbance originates from a large ensemble of unassigned chromophores, which are either intrinsically weak absorbers or present at very low concentrations.

3.2 Assessment of major WBOA chromophores

Fig. 2 presents the optical and chemical characterization of major chromophores in the WBOA sample. Using the same three polarity-based fractions and numerical identifiers as in

Hettiyadura *et al.* (2021),[31] panels (a) and (b) show twenty-three labeled PDA features alongside the EICs of their corresponding compounds. The identified chromophores include furans (#1, C_5H_6O; #3, $C_5H_4O_2$; #8, $C_6H_6O_2$), substituted guaiacols (#24, $C_9H_{12}O_2$; #31, $C_{10}H_{12}O_2$), guaiacol dimers (#27, $C_{16}H_{14}O_4$), and lignin decomposition products (#41, $C_{17}H_{16}O_4$; #43, $C_{18}H_{18}O_4$; #45, $C_{19}H_{20}O_4$), none of which are currently included in the G1–G4 BrC reference mixtures. Although seven PDA features coelute with reference compounds, six of them [#6 ($C_7H_6O_3$), #11 ($C_8H_8O_3$), #19 ($C_9H_6O_2$), #26 ($C_{11}H_{10}O_3$), and #41 ($C_{18}H_{18}O_4$)] exhibit UV-vis absorption spectra that deviate from their assigned references, likely due to coelution with interfering chromophores. Notably, coniferaldehyde (#17; $C_{10}H_{10}O_3$) is the only compound whose PDA spectrum matches that of its reference standard. To improve the comprehensiveness of BrC reference mixtures for future studies, additional inclusion of key chromophores is recommended. These include substituted guaiacols such as 4-ethylguaiacol (#24) and isoeugenol (#31); furans like 1,2-methylfuran (#1); furfural (#3); and 5-methyl-furfural (#8); and lignin-derived benzofuran derivatives (#41, #43, #45). A complete listing of assigned PDA features, UV-vis absorbance spectra, elemental formulas, and plausible structures for the WBOA sample is provided in Table S2 (SI note F).

Comparison of this study with previous measurements from controlled test burns and ambient wood-fueled emissions offers observational insights into the distinct WBOA chemical species reflecting flaming *versus* pyrolysis-dominated conditions. Across both this work and earlier studies,[70,75] oxygenated monoaromatics and lignin decomposition products consistently emerge in high abundance, underscoring their formation irrespective of burning regimes. Secondary plant metabolites such as coumarin and 7-ethoxycoumarin are also detected, indicating their rapid volatilization during thermal
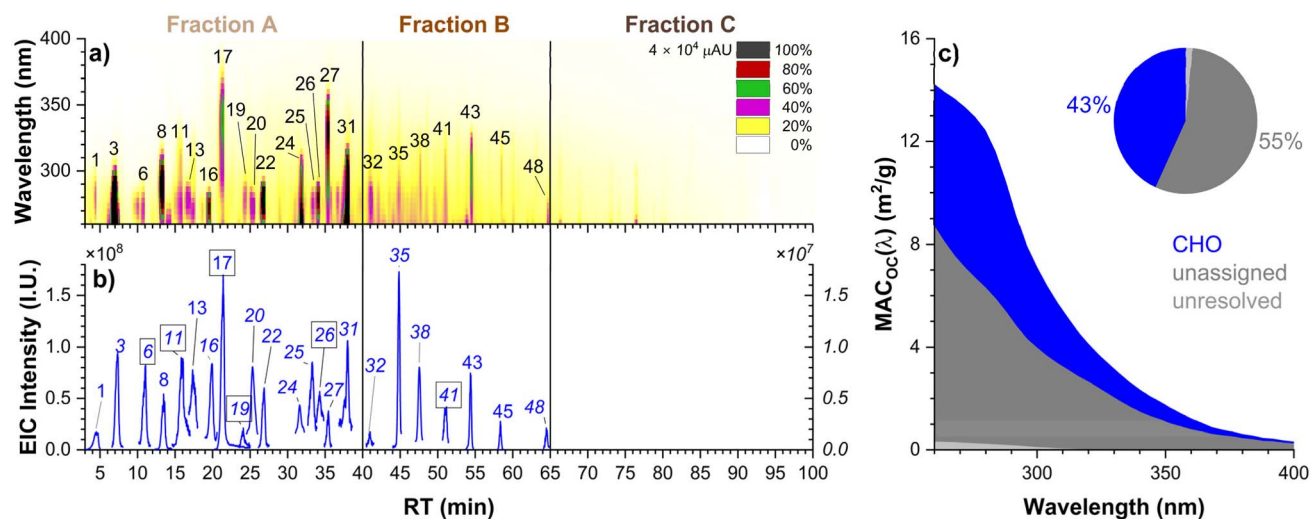
Fig. 2 Characterization of major chromophoric compounds in the WBOA sample. (a) HPLC-PDA absorbance heatmap (b) HPLC-HRMS extracted ion chromatogram overlay, and (c) fractional $MAC_{OC}(\lambda)$ contributions of major WBOA chromophores. Assigned PDA features are numbered in order of retention time and color-coded based on compound class (CHO, blue). Italicized labels indicate MS features with intensities referenced to the right-hand axis; boxed labels denote BrC features matched to compounds in the G1–G4 reference libraries. Assigned CHO compounds contribute up to 43% of total absorbance.

processing.[75] In contrast, flavonoids and their oxygenated derivatives reported in Fleming *et al.* (2020)[75] are absent from the present dataset, suggesting their formation is favored under oxidative conditions of flaming burning. Additionally, nitro-aromatic compounds are absent in this study but were previously observed under elevated NO_x conditions, reinforcing their dependence on NO_x-driven aging. Lastly, large, intact benzofuran derivatives are exclusively detected in this work, indicating their susceptibility to fragmentation in oxygen-rich flaming conditions. These findings highlight the importance of characterizing both flaming- and pyrolysis-driven products to fully realize the chemical variability and atmospheric impacts of WBOA components.

Panel (c) of Fig. 2 shows the contributions of assigned chromophores to the total light absorption in the WBOA sample, expressed as fractions of the $MAC_{OC}(\lambda)$. Compared to the DBOA mixture, the WBOA sample exhibits greater chemical heterogeneity, reflected in the dominance of multiple CHO-class chromophores with a wide range of aromaticity and polarity. Improved chromatographic resolution and more extensive chemical characterization enable attribution of over 43% of total absorbance to identified CHO species, while unresolved components account for only ∼2%. Although 55% of total absorbance remains unassigned, this fraction is notably lower than in the DBOA sample. The higher assignment confidence reflects the expanding body of literature on WBOA composition,[3,31,46] which supports more accurate identification of UV-absorbing chromophores.

3.3 Optical bin classification of DBOA and WBOA mixtures

Fig. 3 compares the optical properties of the DBOA and WBOA mixtures using their representative values of AAE and $\log_{10}(MAC_{OC\_405\ nm})$, shown within the BrC optical classification

framework introduced by Saleh 2020.[4] Reference data for BC[76] and highly absorbing BBOA[77] are included for context. Mean values and standard deviations from triplicate measurements confirm the reproducibility of both AAE and $MAC_{OC\_405\ nm}$ values. For each sample, AAE values calculated across the 280–405 nm and 300–405 nm are consistent, indicating stable spectral behavior in the UV-visible range. The WBOA mixture exhibits a higher AAE (∼12) than DBOA (∼9.5), indicating a steeper wavelength dependence and a greater abundance of
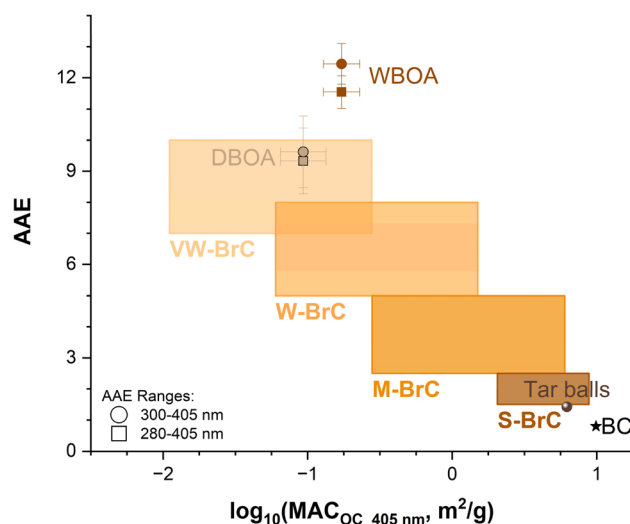

Fig. 3 Classification of WBOA and DBOA mixtures according to the optical framework of Saleh 2020.[4] Average *AAE* and $\log_{10}(MAC_{OC\_405\ nm})$ are calculated for the DBOA and WBOA samples.[44] AAE values are calculated over 280–405 nm (squares) and 300–405 nm (circles) spectral ranges. Reference values for BC[76] and strongly absorbing BrC[77] are included for visual comparison.

strongly absorbing BrC species in the wood-derived sample. Despite this spectral contrast, the two mixtures show comparable absorptivity at 405 nm, with $MAC_{OC\_405\ nm}$ values of 0.172 $m^2\ g^{-1}$ (WBOA) and 0.093 $m^2\ g^{-1}$ (DBOA). Based on $log_{10}(MAC_{OC\_405\ nm})$, both fall between the very weakly (VW–BrC) and weakly (W–BrC) absorbing BrC categories,[4] although their high AAE values are more characteristic of VW–BrC. Upon evaporation, both mixtures are expected to transition toward darker BrC classes,[31,44] with a more pronounced darkening for WBOA due to its lower-volatility, lignin-derived constituents, and likely a weaker effect for the more volatile DBOA mixture.

3.4 Compositional and optical trends of DBOA and WBOA components

Fig. 4 illustrates the pronounced compositional contrasts between the DBOA (panels a and c) and WBOA (panels b and d)

mixtures, as revealed by comparative analysis of ESI(+) high-resolution mass spectra and DBE plots. The DBOA mixture is enriched in lower-molecular-weight RNOCs, primarily in the 80–250 m/z range, consistent with the dominance of chromophore features observed in Fraction A of the HPLC-PDA-HRMS analysis. In contrast, the majority of the WBOA mixture consists of CHO species spanning a broader molecular weight range (80−400 m/z), with a significant fraction of compounds exceeding 250 m/z. These higher-mass CHO species correspond to lignin pyrolysis products and substituted polyaromatics associated with Fractions B and C, hallmarks of pyrolyzed wood biomass. WBOA displays greater molecular diversity and is predominantly composed of highly oxygenated CHO species (74%), many of which exhibit elevated DBE values characteristic of lignocellulosic thermal degradation products. In contrast, the DBOA mixture shows a distinct elemental signature, with only 17% of assigned species falling into the CHO class.
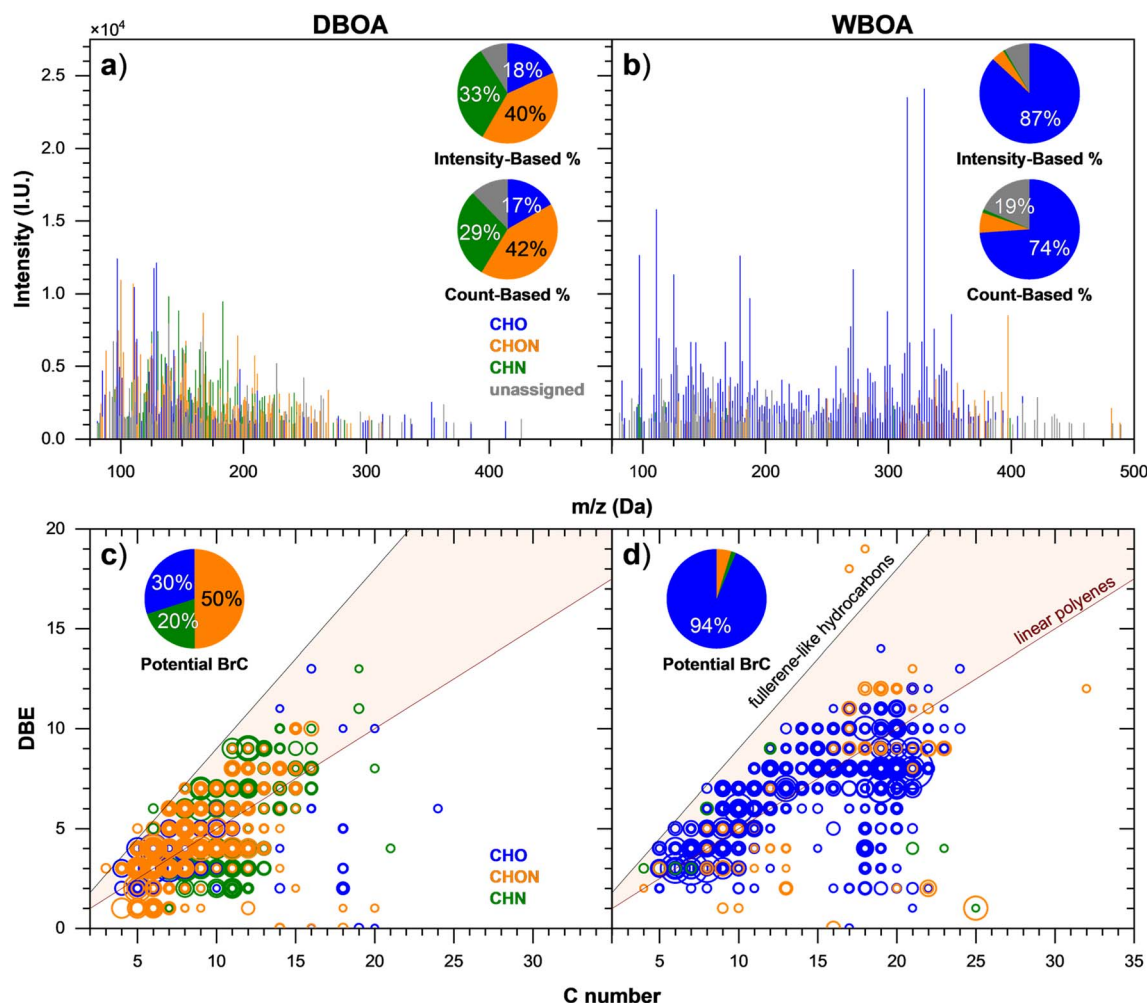

Fig. 4 ESI(+) high-resolution mass spectra and DBE plots of DBOA (a and c) and WBOA (b and d) mixtures. Assigned compounds are color-coded by molecular class (CHO, CHN, CHON), with signal intensities and marker sizes scaled by the square root for better visualization. Pie charts represent the count-weighted and intensity-weighted abundances of molecular classes and unassigned species. In the DBE plots, compounds falling within the shaded region, bounded by the DBE ranges characteristic of fullerene-like hydrocarbons and linear polyenes, are potential BrC chromophores. Pie charts illustrate the relative abundance of potential BrC species resolved by compound class. The WBOA mixture is characterized by a dominant CHO composition, reflecting its lignin-rich nature of wood biomass, while the DBOA mixture is enriched in reduced N-containing species reflecting the composition of dung biofuel.

© 2026 The Author(s). Published by the Royal Society of Chemistry

Environ. Sci.: Atmos., 2026, **6**, 61–75 | **67**

Environmental Science: Atmospheres

Paper

Instead, it is dominated by RNOCs [CHN (29%) and CHON (42%)], many of which are amines, amides, Schiff bases, and N-heterocycles. This RNOCs enrichment reflects both the chemically reduced nature of dung biofuel and the lignin-poor feedstock consumed by cattle, such as wheat, maize straw, and rice straw.[24,62] Overall, the differences in molecular weight distribution, elemental composition, and DBE profiles between DBOA and WBOA mixtures underscore their distinct chemical fingerprints and the strong influence of fuel type on BrC molecular characteristics.

Fig. 4 panels (c) and (d) present DBE plots that visualize the distribution of potential BrC chromophores in the DBOA and WBOA mixtures, respectively. Molecules residing within the shaded region, bounded by DBE values corresponding to linear polyenes (DBE = $0.5 \times$ C number) and fullerene-like hydrocarbons (DBE = $0.9 \times$ C number), exhibit sufficient π-conjugation to absorb light and act as chromophores.[46] In the DBOA mixture, a substantial number of RNOCs (CHON: 50% and CHN: 20%) fall within this region, consistent with the prominent chromophores identified in Fig. 1. In contrast, CHO species dominate this region in the WBOA mixture (94%), aligning with the major chromophores shown in Fig. 2. In both mixtures, approximately 50% of the assigned molecular features fall within the shaded region, indicating that ESI(+) effectively captures a broad range of chromophores. The compositional analysis reinforces that the light-absorbing properties of DBOA are primarily influenced by RNOCs, while those of WBOA are driven by oxidized CHO constituents – reflecting the differing chemical nature of the respective biofuels.

3.5 VBS distributions of DBOA and WBOA components

Fig. 5 illustrates the gas-particle partitioning behavior of the DBOA and WBOA mixtures under varying atmospheric conditions, showcased by two-dimensional heatmaps derived from VBS distributions constructed across a broad range of tOM (1 to 1000 μg m^{-3}) and T (273 to 323 K). Under identical T and tOM conditions, the DBOA mixture shows greater transition to the gas-phase, driven by its enrichment in more volatile components. In contrast, WBOA retains a larger fraction of mass in the particle phase across the same conditions, consistent with its dominance of lower-volatility compounds. As a result, WBOA is more likely to remain in the particle phase for extended atmospheric time, enhancing its persistence, light-absorbing potential, and contribution to radiative energy balance. Conversely, the higher volatility of DBOA constituents promotes more extensive gas-phase transition, facilitating atmospheric transformation into secondary organic aerosol (SOA) products and likely reducing the persistence of its light-absorbing chromophores.

It is worth noting that laboratory-controlled distillation and condensation of biofuel pyrolysis fumes produce complex organic mixtures with components encompassing a wide volatility spectrum, from extremely low-volatility organic compounds (ELVOC) to volatile organic compounds (VOC). Compared to measurements with aerosolized systems, this approach captures a more complete representation of emission constituents, thereby reporting extended VBS distributions that resolve a broader range of gas-particle partitioning under specific T and tOM conditions. The DBOA mixture spans a $\log_{10}(C_T^*)$ range of −4 to 7, with a dominance of intermediate- and volatile organic compounds (IVOC/VOC), which contribute to low particle-phase mass fractions, such as 51% at 298 K and 100 μg m^{-3} tOM or 39% at 323 K and at the same concentration (Fig. S14 and S15). In contrast, for the same conditions of T and tOM, the WBOA components comprise a broader volatility range (−11 to 7), with enhanced contributions from low-volatility (LVOC) and semi-volatile organic compounds (SVOC) which together represent ≥72% of the particle mass (Fig. S14
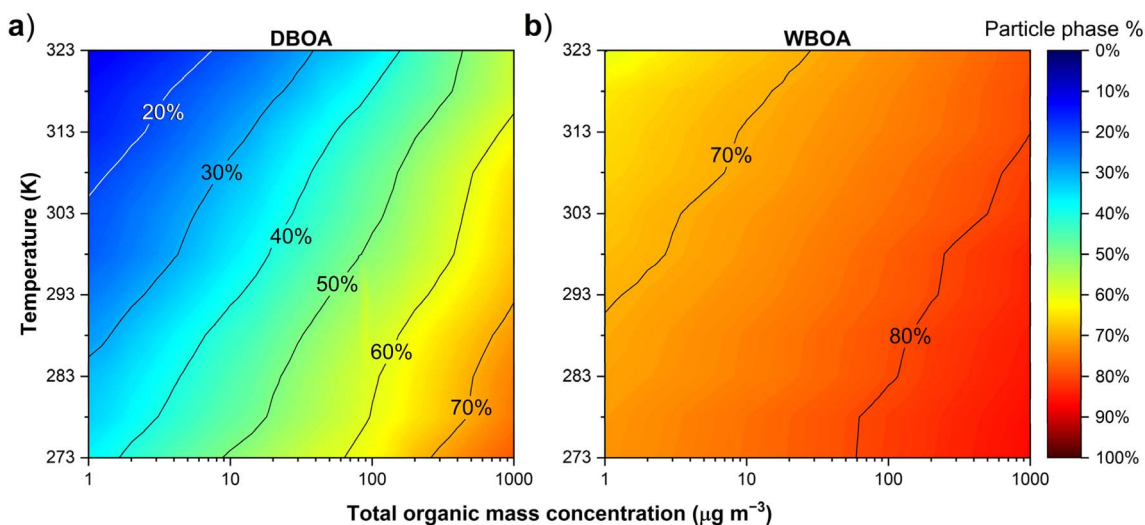

Fig. 5 Calculated particle-phase mass fractions of (a) DBOA and (b) WBOA constituents as a function of tOM and T. Heatmap colors indicate the particle-phase mass fractions. The DBOA mixture shows a greater degree of gas-particle partitioning compared to WBOA, reflecting the higher volatility of its components relative to the less volatile species in the WBOA mixture.

and S15). Masses below 250 m/z, likely monoaromatics, are associated with IVOC/VOC fractions in both mixtures, while 250–400 m/z lignin-derived products in WBOA correspond to LVOC/SVOC constituents.[31] Specific assignments of furan derivatives (DBOA: #73; WBOA: #1, #3, #8) confirm their VOC identity, typically partitioning to the gas-phase unless T is low or tOM is elevated. Conversely, multi-ring benzofuran species (WBOA: #41, #43, and #45), previously detected in bio-oil[78,79] and biochar,[80] behave as persistent LVOC/SVOC species, likely contributing to tar ball formation[81,82] and remaining in the condensed phase across atmospherically relevant T and tOM conditions. Together, these findings underscore the necessity of capturing the full volatility distribution, including VOCs, for accurately modeling gas-particle partitioning in complex aerosolized systems.

4   Atmospheric implications

DBOA emissions containing significant fractions of RNOCs revealed in this report may influence atmospheric chemistry and public health through their high atmospheric reactivity. Semi-volatile RNOCs evaporated from DBOA in aged plumes readily undergo gas-phase oxidation by atmospheric oxidants such as ozone, hydroxyl radicals, and nitrate radicals, forming a variety of secondary nitrogen-containing products (including organonitrates, nitrosamines, and nitramines) some of which exhibit greater toxicological potency than their parent compounds.[69,83–87] These oxidation processes can also release reactive nitrogen species such as NO$_x$, nitrous acid, and nitric acid, thereby reintroducing reactive nitrogen into the atmosphere.[85,88–90] Conversely, the formation of stable organonitrates that repartition into the particle phase can serve as temporary sinks or reservoirs for NO$_x$, impacting the atmospheric nitrogen budget.[91–93] In addition, oxidized RNOCs can contribute to new particle formation and the growth of nitrogen-enriched secondary organic aerosol, potentially influencing cloud condensation nuclei concentrations.[94,95] Their uptake onto wet aerosol particles, cloud, or fog droplets may also perturb acid–base equilibria in aerosol water.[96–98] Many heterocyclic RNOCs act as photosensitizers, facilitating surface-mediated photochemistry in aerosols and aqueous phases.[99,100] While RNOCs are typically considered as short-lived BrC chromophores due to their susceptibility to photobleaching,[101,102] some RNOCs have been shown to increase light absorption upon aging in the presence of NO$_x$, potentially enhancing the optical properties of aged DBOA emissions.[89] Collectively, these processes influence atmospheric oxidant levels, radiative forcing, nitrogen cycling, and air quality – particularly in regions impacted by dung-burning emissions.[11,15,69,84–87] Detailed chemical characterization of DBOA is vital for improving assessments of their environmental and public health impacts and to support the development of effective mitigation strategies in affected communities.

Chemical characterization of thermal degradation products formed under pyrolytic conditions reveals key precursor compounds and structural motifs, such as RNOCs and oxygenated aromatics, that will further transform under oxidative environments. Identification of these core molecular species in pyrolytic DBOA and their volatility profiles provides a mechanistic foundation for modeling predictions of their evolution during smoldering and flaming burning, where oxygen availability and higher temperatures drive radical chemistry reactions leading to oxidation, nitration, and fragmentation. Understanding the precursors formed under pyrolysis thus provides a mechanistic basis for reconstructing more complex emission profiles and for tracking transformation pathways of key emitted products. Such knowledge may guide the design of future burning experiments, inform fuel- and regime-specific parameterizations, and facilitate prediction of BrC reactivity and transformations, radiative forcing, and public health impacts in regions affected by DBOA emissions.

Author contributions

D. C.-A. and A. L. designed the study. B. S. collected the dung cake samples and contributed to study conceptualization and data interpretation. S. M. K., A. M. S., J. E., L. E., J. K., J. W., K. H., and N. H. assisted with laboratory experiments. D. C.-A. and S. S. performed molecular characterization analyses. D. C.-A. and A. L. wrote the manuscript with contributions from all co-authors. A. L. secured grant funding for this study and directed the overall project.

Conflicts of interest

There are no conflicts to declare.

Data availability

The data supporting this article have been included as part of supplementary information (SI). Supplementary information: SI note A and Fig. S1 show the starting dung cake starting materials and describe the details of generating the DBOA mixture. SI note B and Fig. S2 explain the steps taken to estimate OC mass-to-sample mass ratios in the two samples. SI note C provides a detailed summary of the operative parameters set to conduct HPLC-PDA-HRMS analysis. SI note D and Fig. S3 outline the AAE linear curve fitting analysis for the two mixtures. SI note E and Fig. S4 provide details on EIC generation using MZmine 2.53 and representative ESI/APPI(±) high-resolution mass spectra for DBOA and WBOA mixtures. Fig. S5 and S6 present comparative analyses of shared and unique masses detected in ESI(+), APPI(+), and both modes. SI note F describes the procedures taken to characterize major BrC chromophores present in the DBOA and WBOA mixtures. Fig. S7 displays HPLC-PDA chromatograms depicting the assigned PDA features of special focus in this study. Fig. S8–S10 illustrate assigned PDA features and corresponding EICs for DBOA, Fraction A WBOA, and Fraction B WBOA mixtures. Tables S1 and S2 outline PDA feature retention times, experimental UV-vis absorbance spectra, observed m/z values, and plausible structures of BrC chromophores and reference compounds for DBOA and WBOA, respectively. SI note G provides details on general molecular trends for the DBOA and

© 2026 The Author(s). Published by the Royal Society of Chemistry

Environ. Sci.: Atmos., 2026, **6**, 61–75 | **69**

WBOA samples. Fig. S11 illustrates DBE distributions of all species in ionization modes. Fig. S12 conveys comparative analyses of species and potential BrC chromophores detected in APPI(+) mode for both samples. Fig. S13 displays VK diagrams of detected DBOA and WBOA components. SI note H outlines the sequence of calculations followed to generate VBS diagrams of the two mixtures. Fig. S14 and S15 convey the concentration-driven and temperature-driven gas-particle partitioning behaviors for both mixtures. Fig. S16 illustrates additional two-dimensional heatmaps to visualize upper-limit partitioning trends. See DOI: **https://doi.org/10.1039/d5ea00105f**.

Acknowledgements

References

1 T. C. Bond and R. W. Bergstrom, Light Absorption by Carbonaceous Particles: An Investigative Review, *Aerosol Sci. Technol.*, 2006, **40**(1), 27–67, DOI: **10.1080/02786820500421521**.

2 A. Laskin, J. Laskin and S. A. Nizkorodov, Chemistry of Atmospheric Brown Carbon, *Chem. Rev.*, 2015, **115**(10), 4335–4382, DOI: **10.1021/cr5006167**.

3 A. Laskin, C. P. West and A. P. S. Hettiyadura, Molecular Insights into the Composition, Sources, and Aging of Atmospheric Brown Carbon, *Chem. Soc. Rev.*, 2025, **54**(3), 1583–1612, DOI: **10.1039/D3CS00609C**.

4 R. Saleh, From Measurements to Models: Toward Accurate Representation of Brown Carbon in Climate Calculations, *Curr. Pollut. Rep.*, 2020, **6**(2), 90–104, DOI: **10.1007/s40726-020-00139-3**.

5 M. O. Andreae and A. Gelencsér, Black Carbon or Brown Carbon? The Nature of Light-Absorbing Carbonaceous Aerosols, *Atmos. Chem. Phys.*, 2006, **6**(10), 3131–3148, DOI: **10.5194/acp-6-3131-2006**.

6 J. Yan, X. Wang, P. Gong, C. Wang and Z. Cong, Review of Brown Carbon Aerosols: Recent Progress and Perspectives, *Sci. Total Environ.*, 2018, **634**, 1475–1485, DOI: **10.1016/j.scitotenv.2018.04.083**.

7 Intergovernmental Panel On Climate Change (Ipcc), *Climate Change 2021 – the Physical Science Basis: Working Group I Contribution to the Sixth Assessment Report of the Intergovernmental Panel on Climate Change*, 1st edn, Cambridge University Press, 2023, DOI: **10.1017/9781009157896**.

8 M. O. Andreae, Emission of Trace Gases and Aerosols from Biomass Burning – an Updated Assessment, *Atmos. Chem. Phys.*, 2019, **19**(13), 8523–8546, DOI: **10.5194/acp-19-8523-2019**.

9 M. Shrivastava, S. Lou, A. Zelenyuk, R. C. Easter, R. A. Corley, B. D. Thrall, P. J. Rasch, J. D. Fast, S. L. Massey Simonich, H. Shen and S. Tao, Global Long-Range Transport and Lung Cancer Risk from Polycyclic Aromatic Hydrocarbons Shielded by Coatings of Organic Aerosol, *Proc. Natl. Acad. Sci. U. S. A.*, 2017, **114**(6), 1246–1251, DOI: **10.1073/pnas.1618475114**.

10 M. Romanello, M. Walawender, S.-C. Hsu, A. Moskeland, Y. Palmeiro-Silva, D. Scamman, Z. Ali, N. Ameli, D. Angelova, S. Ayeb-Karlsson, S. Basart, J. Beagley, P. J. Beggs, L. Blanco-Villafuerte, W. Cai, M. Callaghan, D. Campbell-Lendrum, J. D. Chambers, V. Chicmana-Zapata, L. Chu, T. J. Cross, K. R. Van Daalen, C. Dalin, N. Dasandi, S. Dasgupta, M. Davies, R. Dubrow, M. J. Eckelman, J. D. Ford, C. Freyberg, O. Gasparyan, G. Gordon-Strachan, M. Grubb, S. H. Gunther, I. Hamilton, Y. Hang, R. Hänninen, S. Hartinger, K. He, J. Heidecke, J. J. Hess, L. Jamart, S. Jankin, H. Jatkar, O. Jay, I. Kelman, H. Kennard, G. Kiesewetter, P. Kinney, D. Kniveton, R. Kouznetsov, P. Lampard, J. K. W. Lee, B. Lemke, B. Li, Y. Liu, Z. Liu, A. Llabrés-Brustenga, M. Lott, R. Lowe, J. Martinez-Urtaza, M. Maslin, L. McAllister, C. McMichael, Z. Mi, J. Milner, K. Minor, J. Minx, N. Mohajeri, N. C. Momen, M. Moradi-Lakeh, K. Morrisey, S. Munzert, K. A. Murray, N. Obradovich, M. B. O'Hare, C. Oliveira, T. Oreszczyn, M. Otto, F. Owfi, O. L. Pearman, F. Pega, A. J. Perishing, A.-C. Pinho-Gomes, J. Ponmattam, M. Rabbaniha, J. Rickman, E. Robinson, J. Rocklöv, D. Rojas-Rueda, R. N. Salas, J. C. Semenza, J. D. Sherman, J. Shumake-Guillemot, P. Singh, H. Sjödin, J. Slater, M. Sofiev, C. Sorensen, M. Springmann, Z. Stalhandske, J. D. Stowell, M. Tabatabaei, J. Taylor, D. Tong, C. Tonne, M. Treskova, J. A. Trinanes, A. Uppstu, F. Wagner, L. Warnecke, H. Whitcombe, P. Xian, C. Zavaleta-Cortijo, C. Zhang, R. Zhang, S. Zhang, Y. Zhang, Q. Zhu, P. Gong, H. Montgomery and A. Costello, The 2024 Report of the Lancet Countdown on Health and Climate Change: Facing Record-Breaking Threats from Delayed Action, *Lancet*, 2024, **404**(10465), 1847–1896, DOI: **10.1016/S0140-6736(24)01822-1**.

11 B. Rooney, R. Zhao, Y. Wang, K. H. Bates, A. Pillarisetti, S. Sharma, S. Kundu, T. C. Bond, N. L. Lam, B. Ozaltun, L. Xu, V. Goel, L. T. Fleming, R. Weltman, S. Meinardi, D. R. Blake, S. A. Nizkorodov, R. D. Edwards, A. Yadav, N. K. Arora, K. R. Smith and J. H. Seinfeld, Impacts of Household Sources on Air Pollution at Village and Regional Scales in India, *Atmos. Chem. Phys.*, 2019, **19**(11), 7719–7742, DOI: **10.5194/acp-19-7719-2019**.

12 K. Skyllakou, M.-B. Korras-Carraca, C. Matsoukas, N. Hatzianastassiou, S. N. Pandis and A. Nenes, Predicted Concentrations and Optical Properties of Brown Carbon from Biomass Burning over Europe, *ACS EST Air*, 2024, 714–725, DOI: **10.1021/acsestair.4c00032**.

13 M. A. DeLessio, K. Tsigaridis, S. E. Bauer, J. Chowdhary and G. L. Schuster, Modeling Atmospheric Brown Carbon in the GISS ModelE Earth System Model, *Atmos. Chem. Phys.*, 2024, **24**(10), 6275–6304, DOI: **10.5194/acp-24-6275-2024**.

14 M. Loebel Roson, R. Duruisseau-Kuntz, M. Wang, K. Klimchuk, R. J. Abel, J. J. Harynuk and R. Zhao,

Chemical Characterization of Emissions Arising from Solid Fuel Combustion—Contrasting Wood and Cow Dung Burning, *ACS Earth Space Chem.*, 2021, **5**(10), 2925–2937, DOI: **10.1021/acsearthspacechem.1c00268**.

15 A. Pandey, A. Hsu, S. Tiwari, S. Pervez and R. K. Chakrabarty, Light Absorption by Organic Aerosol Emissions Rivals That of Black Carbon from Residential Biomass Fuels in South Asia, *Environ. Sci. Technol. Lett.*, 2020, **7**(4), 266–272, DOI: **10.1021/acs.estlett.0c00058**.

16 World Bank, *2025 Tracking SDG 7: The Energy Progress Report*, Chapter 2 Access to Clean Cooking, Washington, DC, USA, 2025.

17 E. Kassianov, C. J. Flynn, J. C. Barnard, L. K. Berg, S. J. Beus, X. Chen, S. China, J. M. Comstock, B. D. Ermold, A. A. Fakoya, G. Kulkarni, N. N. Lata, N. G. Mcdowell, V. R. Morris, M. S. Pekour, H. J. Rasmussen, L. D. Riihimaki, M. Shi, M. Shrivastava, H. Telg, A. Zelenyuk and D. Zhang, Radiative Impact of Record-Breaking Wildfires from Integrated Ground-Based Data, *Sci. Rep.*, 2025, **15**(1), 8262, DOI: **10.1038/s41598-025-85103-1**.

18 C. A. Kolden, J. T. Abatzoglou, M. W. Jones and P. Jain, Wildfires in 2024, *Nat. Rev. Earth Environ.*, 2025, **6**(4), 237–239, DOI: **10.1038/s43017-025-00663-0**.

19 H. Brown, X. Liu, Y. Feng, Y. Jiang, M. Wu, Z. Lu, C. Wu, S. Murphy and R. Pokhrel, Radiative Effect and Climate Impacts of Brown Carbon with the Community Atmosphere Model (CAM5), *Atmos. Chem. Phys.*, 2018, **18**(24), 17745–17768, DOI: **10.5194/acp-18-17745-2018**.

20 P. Tuccella, L. Di Antonio, A. Di Muzio, V. Colaiuda, R. Lidori, L. Menut, G. Pitari and E. Raparelli, Modeling the Black and Brown Carbon Absorption and Their Radiative Impact: The June 2023 Intense Canadian Boreal Wildfires Case Study, *J. Geophys. Res. Atmospheres*, 2025, **130**(7), e2024JD042674, DOI: **10.1029/2024JD042674**.

21 Y. Han, J. Cai, Y. Chen, Y. Zhang, L. N. Jin, T. Chen, J. Li, G. Zhang and J. Chen, Concurrent Formation of Low-Maturity EC and BrC in Biomass and Coal Burning: O-PAH as a Precursor, *Environ. Sci. Technol.*, 2025, **59**(24), 12083–12095, DOI: **10.1021/acs.est.4c13299**.

22 R. Saleh, Z. Cheng and K. Atwi, The Brown–Black Continuum of Light-Absorbing Combustion Aerosols, *Environ. Sci. Technol. Lett.*, 2018, **5**(8), 508–513, DOI: **10.1021/acs.estlett.8b00305**.

23 M. Loebel Roson, S. A. Schmidt, V. Choudhary, T. A. Johnson, A. P. de la Mata, J. J. Harynuk and R. Zhao, Comprehensive Analysis of Emissions from Wood and Cow Dung Burning Using Chemometrics and Two-Dimensional Gas Chromatography, *Chemosphere*, 2024, **366**, 143445, DOI: **10.1016/j.chemosphere.2024.143445**.

24 R. J. Sheesley, J. J. Schauer, Z. Chowdhury, G. R. Cass and B. R. T. Simoneit, Characterization of Organic Aerosols Emitted from the Combustion of Biomass Indigenous to South Asia, *J. Geophys. Res. Atmospheres*, 2003, **108**(D9), 2002JD002981, DOI: **10.1029/2002JD002981**.

25 V. Moschos, C. Christensen, M. Mouton, M. N. Fiddler, T. Isolabella, F. Mazzei, D. Massabò, B. J. Turpin, S. Bililign and J. D. Surratt, Quantifying the Light-Absorption Properties and Molecular Composition of Brown Carbon Aerosol from Sub-Saharan African Biomass Combustion, *Environ. Sci. Technol.*, 2024, **58**(9), 4268–4280, DOI: **10.1021/acs.est.3c09378**.

26 R. F. Hems, E. G. Schnitzler, C. Liu-Kang, C. D. Cappa and J. P. D. Abbatt, Aging of Atmospheric Brown Carbon Aerosol, *ACS Earth Space Chem.*, 2021, **5**(4), 722–748, DOI: **10.1021/acsearthspacechem.0c00346**.

27 C. George, M. Ammann, B. D'Anna, D. J. Donaldson and S. A. Nizkorodov, Heterogeneous Photochemistry in the Atmosphere, *Chem. Rev.*, 2015, **115**(10), 4218–4258, DOI: **10.1021/cr500648z**.

28 A. L. Hodshire, A. Akherati, M. J. Alvarado, B. Brown-Steiner, S. H. Jathar, J. L. Jimenez, S. M. Kreidenweis, C. R. Lonsdale, T. B. Onasch, A. M. Ortega and J. R. Pierce, Aging Effects on Biomass Burning Aerosol Mass and Composition: A Critical Review of Field and Laboratory Studies, *Environ. Sci. Technol.*, 2019, **53**(17), 10007–10022, DOI: **10.1021/acs.est.9b02588**.

29 C. Warneke, J. P. Schwarz, J. Dibb, O. Kalashnikova, G. Frost, J. Al-Saad, S. S. Brown, Wm. A. Brewer, A. Soja, F. C. Seidel, R. A. Washenfelder, E. B. Wiggins, R. H. Moore, B. E. Anderson, C. Jordan, T. I. Yacovitch, S. C. Herndon, S. Liu, T. Kuwayama, D. Jaffe, N. Johnston, V. Selimovic, R. Yokelson, D. M. Giles, B. N. Holben, P. Goloub, I. Popovici, M. Trainer, A. Kumar, R. B. Pierce, D. Fahey, J. Roberts, E. M. Gargulinski, D. A. Peterson, X. Ye, L. H. Thapa, P. E. Saide, C. H. Fite, C. D. Holmes, S. Wang, M. M. Coggon, Z. C. J. Decker, C. E. Stockwell, L. Xu, G. Gkatzelis, K. Aikin, B. Lefer, J. Kaspari, D. Griffin, L. Zeng, R. Weber, M. Hastings, J. Chai, G. M. Wolfe, T. F. Hanisco, J. Liao, P. Campuzano Jost, H. Guo, J. L. Jimenez and J. Crawford, The FIREX-AQ Science Team. Fire Influence on Regional to Global Environments and Air Quality (FIREX-AQ), *J. Geophys. Res. Atmospheres*, 2023, **128**(2), e2022JD037758, DOI: **10.1029/2022JD037758**.

30 R. A. Washenfelder, L. Azzarello, K. Ball, S. S. Brown, Z. C. J. Decker, A. Franchin, C. D. Fredrickson, K. Hayden, C. D. Holmes, A. M. Middlebrook, B. B. Palm, R. B. Pierce, D. J. Price, J. M. Roberts, M. A. Robinson, J. A. Thornton, C. C. Womack and C. J. Young, Complexity in the Evolution, Composition, and Spectroscopy of Brown Carbon in Aircraft Measurements of Wildfire Plumes, *Geophys. Res. Lett.*, 2022, **49**(9), e2022GL098951, DOI: **10.1029/2022GL098951**.

31 A. P. S. Hettiyadura, V. Garcia, C. Li, C. P. West, J. Tomlin, Q. He, Y. Rudich and A. Laskin, Chemical Composition and Molecular-Specific Optical Properties of Atmospheric Brown Carbon Associated with Biomass Burning, *Environ. Sci. Technol.*, 2021, **55**(4), 2511–2521, DOI: **10.1021/acs.est.0c05883**.

32 K. Siemens, T. Paik, A. Li, F. Rivera-Adorno, J. Tomlin, Q. Xie, R. K. Chakrabarty and A. Laskin, Light Absorption and Chemical Composition of Brown Carbon Organic Aerosol Produced from Burning of Selected Biofuels, *ACS*

© 2026 The Author(s). Published by the Royal Society of Chemistry

Environ. Sci.: Atmos., 2026, **6**, 61–75 | 71

Earth Space Chem., 2024, **8**(7), 1416–1428, DOI: **10.1021/acsearthspacechem.4c00056**.

33 Y. Huang, X. Li, D. D. Huang, R. Lei, B. Zhou, Y. Zhang and X. Ge, *Machine Learning Assisted Chemical Characterization and Optical Properties of Atmospheric Brown Carbon in Nanjing*, China, 2024, DOI: **10.5194/egusphere-2024-2757**.

34 Y. Wang, R.-J. Huang, H. Zhong, T. Wang, L. Yang, W. Yuan, W. Xu and Z. An, Predictions of the Optical Properties of Brown Carbon Aerosol by Machine Learning with Typical Chromophores, *Environ. Sci. Technol.*, 2024, **58**(46), 20588–20597, DOI: **10.1021/acs.est.4c09031**.

35 F. Wang, Z. Lu, G. Lin, G. R. Carmichael and M. Gao, Brown Carbon in East Asia: Seasonality, Sources, and Influences on Regional Climate and Air Quality, *ACS Environ. Au*, 2025, **5**(1), 128–137, DOI: **10.1021/acsenvironau.4c00080**.

36 C. Navinya, T. S. Kapoor, G. Anurag, C. Venkataraman, H. C. Phuleria and R. K. Chakrabarty, Brownness of Organics in Anthropogenic Biomass Burning Aerosols over South Asia, *Atmos. Chem. Phys.*, 2024, **24**(23), 13285–13297, DOI: **10.5194/acp-24-13285-2024**.

37 C. Navinya, T. S. Kapoor, C. Venkataraman, H. C. Phuleria and R. K. Chakrabarty, Brown Carbon Light Absorption over India: Research Status and Need for Discerning Climate Impacts, *ACS EST Air*, 2025, **2**(7), 1115–1135, DOI: **10.1021/acsestair.5c00010**.

38 O. Stoner, J. Lewis, I. L. Martínez, S. Gumy, T. Economou and H. Adair-Rohani, Household Cooking Fuel Estimates at Global and Country Level for 1990 to 2030, *Nat. Commun.*, 2021, **12**(1), 5793, DOI: **10.1038/s41467-021-26036-x**.

39 T. Wang, J. Zhang, H. Lamkaddam, K. Li, K. Y. Cheung, L. Kattner, E. Gammelsæter, M. Bauer, Z. C. J. Decker, D. Bhattu, R. Huang, R. L. Modini, J. G. Slowik, I. El Haddad, A. S. H. Prevot and D. M. Bell, Chemical Characterization of Organic Vapors from Wood, Straw, Cow Dung, and Coal Burning, *Atmos. Chem. Phys.*, 2025, **25**(4), 2707–2724, DOI: **10.5194/acp-25-2707-2025**.

40 M. G. Adam, P. T. M. Tran, N. Bolan and R. Balasubramanian, Biomass Burning-Derived Airborne Particulate Matter in Southeast Asia: A Critical Review, *J. Hazard. Mater.*, 2021, **407**, 124760, DOI: **10.1016/j.jhazmat.2020.124760**.

41 K. He, Z. Shen, L. Zhang, X. Wang, B. Zhang, J. Sun, H. Xu, S. S. Hang Ho and J. Cao, Emission of Intermediate Volatile Organic Compounds from Animal Dung and Coal Combustion and Its Contribution to Secondary Organic Aerosol Formation in Qinghai-Tibet Plateau, China, *Environ. Sci. Technol.*, 2024, **58**(25), 11118–11127, DOI: **10.1021/acs.est.4c02618**.

42 J. Zhang, K. Li, T. Wang, E. Gammelsæter, R. K. Y. Cheung, M. Surdu, S. Bogler, D. Bhattu, D. S. Wang, T. Cui, L. Qi, H. Lamkaddam, I. El Haddad, J. G. Slowik, A. S. H. Prevot and D. M. Bell, Bulk and Molecular-Level Composition of Primary Organic Aerosol from Wood, Straw, Cow Dung, and Plastic Burning, *Atmos. Chem. Phys.*, 2023, **23**(22), 14561–14576, DOI: **10.5194/acp-23-14561-2023**.

43 J. S. Fu, N. C. Hsu, Y. Gao, K. Huang, C. Li, N.-H. Lin and S.-C. Tsay, Evaluating the Influences of Biomass Burning during 2006 BASE-ASIA: A Regional Chemical Transport Modeling, *Atmos. Chem. Phys.*, 2012, **12**(9), 3837–3855, DOI: **10.5194/acp-12-3837-2012**.

44 D. Calderon-Arrieta, A. C. Morales, A. P. S. Hettiyadura, T. M. Estock, C. Li, Y. Rudich and A. Laskin, Enhanced Light Absorption and Elevated Viscosity of Atmospheric Brown Carbon through Evaporation of Volatile Components, *Environ. Sci. Technol.*, 2024, **58**(17), 7493–7504, DOI: **10.1021/acs.est.3c10184**.

45 R. Godec, K. Longmont and R. Hutte, *Method and Apparatus for The Measurement of Dissolved Carbon*, 1999, vol. 5, p. , p. 902. **https://patentimages.storage.googleapis.com/0d/73/ed/9eab5b71f8a4ae/US5902751**.

46 P. Lin, L. T. Fleming, S. A. Nizkorodov, J. Laskin and A. Laskin, Comprehensive Molecular Characterization of Atmospheric Brown Carbon by High Resolution Mass Spectrometry with Electrospray and Atmospheric Pressure Photoionization, *Anal. Chem.*, 2018, **90**(21), 12493–12502, DOI: **10.1021/acs.analchem.8b02177**.

47 A. Laskin, J. S. Smith and J. Laskin, Molecular Characterization of Nitrogen-Containing Organic Compounds in Biomass Burning Aerosols Using High-Resolution Mass Spectrometry, *Environ. Sci. Technol.*, 2009, **43**(10), 3764–3771, DOI: **10.1021/es803456n**.

48 Y. Lin, X. Zhang, L. Li, Z. Li, R. Wang, S. Xing and Y. Han, Review on the Molecular Characterization of Atmospheric Organic Aerosols Using High-Resolution Orbitrap Mass Spectrometry: Techniques, Applications, and Perspectives, *Aerosol Sci. Eng.*, 2025, DOI: **10.1007/s41810-025-00332-1**.

49 M. Pelillo, M. E. Cuvelier, B. Biguzzi, T. Gallina Toschi, C. Berset and G. Lercker, Calculation of the Molar Absorptivity of Polyphenols by Using Liquid Chromatography with Diode Array Detection: The Case of Carnosic Acid, *J. Chromatogr. A*, 2004, **1023**(2), 225–229, DOI: **10.1016/S0021-9673(03)01206-8**.

50 R. Schmid, S. Heuckeroth, A. Korf, A. Smirnov, O. Myers, T. S. Dyrlund, R. Bushuiev, K. J. Murray, N. Hoffmann, M. Lu, A. Sarvepalli, Z. Zhang, M. Fleischauer, K. Dührkop, M. Wesner, S. J. Hoogstra, E. Rudt, O. Mokshyna, C. Brungs, K. Ponomarov, L. Mutabdžija, T. Damiani, C. J. Pudney, M. Earll, P. O. Helmer, T. R. Fallon, T. Schulze, A. Rivas-Ubach, A. Bilbao, H. Richter, L.-F. Nothias, M. Wang, M. Orešič, J.-K. Weng, S. Böcker, A. Jeibmann, H. Hayen, U. Karst, P. C. Dorrestein, D. Petras, X. Du and T. Pluskal, Integrative Analysis of Multimodal Mass Spectrometry Data in MZmine 3, *Nat. Biotechnol.*, 2023, **41**(4), 447–449, DOI: **10.1038/s41587-023-01690-2**.

51 P. J. Roach, J. Laskin and A. Laskin, Higher-Order Mass Defect Analysis for Mass Spectra of Complex Organic Mixtures, *Anal. Chem.*, 2011, **83**(12), 4924–4929, DOI: **10.1021/ac200654j**.

52 V. Krevelen, Graphical-Statistical Method for the Study of Structure and Reaction Processes of Coal, *Fuel*, 1950, **29**, 269–284.

53 F. W. McLafferty and F. Tureček, *Interpretation of Mass Spectra*, 4th edn, University Science Books, Mill Valley, Calif, 1993.

54 N. M. Donahue, J. H. Kroll, S. N. Pandis and A. L. Robinson, A Two-Dimensional Volatility Basis Set – Part 2: Diagnostics of Organic-Aerosol Evolution, *Atmos. Chem. Phys.*, 2012, **12**(2), 615–634, DOI: **10.5194/acp-12-615-2012**.

55 N. M. Donahue, S. A. Epstein, S. N. Pandis and A. L. Robinson, A Two-Dimensional Volatility Basis Set: 1. Organic-Aerosol Mixing Thermodynamics, *Atmos. Chem. Phys.*, 2011, **11**(7), 3303–3318, DOI: **10.5194/acp-11-3303-2011**.

56 Y. Li, U. Pöschl and M. Shiraiwa, Molecular Corridors and Parameterizations of Volatility in the Chemical Evolution of Organic Aerosols, *Atmos. Chem. Phys.*, 2016, **16**(5), 3327–3344, DOI: **10.5194/acp-16-3327-2016**.

57 Q. Xie, N. G. A. Gerrebos, D. Calderon-Arrieta, I. S. Morton, E. R. Halpern, C. Li, M. F. Zeng, A. K. Bertram, Y. Rudich and A. Laskin, Molecular Insights into Gas–Particle Partitioning and Viscosity of Atmospheric Brown Carbon, *Environ. Sci. Technol.*, 2024, **58**(41), 18284–18294, DOI: **10.1021/acs.est.4c05650**.

58 D. Calderon-Arrieta, J. Knull, Q. Xie, C. Li, J. Wang, L. Evans, N. Hajian, K. Hill, Y. Rudich and A. Laskin, Photolytic Transformation of Soluble and Colloidal Components in Atmospheric Brown Carbon, *ACS EST Air*, 2025, DOI: **10.1021/acsestair.5c00301**.

59 M. Ranjan, A. A. Presto, A. A. May and A. L. Robinson, Temperature Dependence of Gas–Particle Partitioning of Primary Organic Aerosol Emissions from a Small Diesel Engine, *Aerosol Sci. Technol.*, 2012, **46**(1), 13–21, DOI: **10.1080/02786826.2011.602761**.

60 Q. Xie, E. Windwer, I. S. Morton, K. E. Lavin, E. R. Halpern, D. Nissenbaum, S. A. Nizkorodov, Y. Rudich and A. Laskin, Molecular Characterization of Composition and Volatility of Ambient Organic Aerosol Sampled by an UAV-Mounted Portable Aethalometer, *Anal. Chem.*, 2025, **97**(32), 17743–17751, DOI: **10.1021/acs.analchem.5c03027**.

61 S. A. Epstein, I. Riipinen and N. M. Donahue, A Semiempirical Correlation between Enthalpy of Vaporization and Saturation Concentration for Organic Aerosol, *Environ. Sci. Technol.*, 2010, **44**(2), 743–748, DOI: **10.1021/es902497z**.

62 P. Binod, R. Sindhu, R. R. Singhania, S. Vikram, L. Devi, S. Nagalakshmi, N. Kurien, R. K. Sukumaran and A. Pandey, Bioethanol Production from Rice Straw: An Overview, *Bioresour. Technol.*, 2010, **101**(13), 4767–4774, DOI: **10.1016/j.biortech.2009.10.079**.

63 M. Claeys, R. Vermeylen, F. Yasmeen, Y. Gómez-González, X. Chi, W. Maenhaut, T. Mészáros and I. Salma, Chemical Characterisation of Humic-like Substances from Urban, Rural and Tropical Biomass Burning Environments Using Liquid Chromatography with UV/Vis Photodiode Array Detection and Electrospray Ionisation Mass Spectrometry, *Environ. Chem.*, 2012, **9**(3), 273, DOI: **10.1071/EN11163**.

64 X. Wang, R. Gu, L. Wang, W. Xu, Y. Zhang, B. Chen, W. Li, L. Xue, J. Chen and W. Wang, Emissions of Fine Particulate Nitrated Phenols from the Burning of Five Common Types of Biomass, *Environ. Pollut.*, 2017, **230**, 405–412, DOI: **10.1016/j.envpol.2017.06.072**.

65 C. Mohr, F. D. Lopez-Hilfiker, P. Zotter, A. S. H. Prévôt, L. Xu, N. L. Ng, S. C. Herndon, L. R. Williams, J. P. Franklin, M. S. Zahniser, D. R. Worsnop, W. B. Knighton, A. C. Aiken, K. J. Gorkowski, M. K. Dubey, J. D. Allan and J. A. Thornton, Contribution of Nitrated Phenols to Wood Burning Brown Carbon Light Absorption in Detling, United Kingdom during Winter Time, *Environ. Sci. Technol.*, 2013, **47**(12), 6316–6324, DOI: **10.1021/es400683v**.

66 R. F. Hems and J. P. D. Abbatt, Aqueous Phase Photo-Oxidation of Brown Carbon Nitrophenols: Reaction Kinetics, Mechanism, and Evolution of Light Absorption, *ACS Earth Space Chem.*, 2018, **2**(3), 225–234, DOI: **10.1021/acsearthspacechem.7b00123**.

67 D. Wang, Z. Shen, G. Bai, L. Zhang, S. Huang, H. Zheng, C. Li, J. Sun, H. Xu and J. Cao, Oxidized Nitrogen-Containing Organic Compounds Formation Enhanced the Light Absorption of $PM_{2.5}$ Brown Carbon, *J. Geophys. Res. Atmospheres*, 2025, **130**(3), e2024JD042960, DOI: **10.1029/2024JD042960**.

68 M. Zhang, D. Cai, J. Lin, Z. Liu, M. Li, Y. Wang and J. Chen, Molecular Characterization of Atmospheric Organic Aerosols in Typical Megacities in China, *Npj Clim. Atmospheric Sci.*, 2024, **7**(1), 230, DOI: **10.1038/s41612-024-00784-1**.

69 L. T. Fleming, R. Weltman, A. Yadav, R. D. Edwards, N. K. Arora, A. Pillarisetti, S. Meinardi, K. R. Smith, D. R. Blake and S. A. Nizkorodov, Emissions from Village Cookstoves in Haryana, India, and Their Potential Impacts on Air Quality, *Atmos. Chem. Phys.*, 2018, **18**(20), 15169–15182, DOI: **10.5194/acp-18-15169-2018**.

70 L. T. Fleming, P. Lin, A. Laskin, J. Laskin, R. Weltman, R. D. Edwards, N. K. Arora, A. Yadav, S. Meinardi, D. R. Blake, A. Pillarisetti, K. R. Smith and S. A. Nizkorodov, Molecular Composition of Particulate Matter Emissions from Dung and Brushwood Burning Household Cookstoves in Haryana, India, *Atmos. Chem. Phys.*, 2018, **18**(4), 2461–2480, DOI: **10.5194/acp-18-2461-2018**.

71 G. J. Stewart, W. J. F. Acton, B. S. Nelson, A. R. Vaughan, J. R. Hopkins, R. Arya, A. Mondal, R. Jangirh, S. Ahlawat, L. Yadav, S. K. Sharma, R. E. Dunmore, S. S. M. Yunus, C. N. Hewitt, E. Nemitz, N. Mullinger, R. Gadi, L. K. Sahu, N. Tripathi, A. R. Rickard, J. D. Lee, T. K. Mandal and J. F. Hamilton, Emissions of Non-Methane Volatile Organic Compounds from Combustion of Domestic Fuels in Delhi, India, *Atmos. Chem. Phys.*, 2021, **21**(4), 2383–2406, DOI: **10.5194/acp-21-2383-2021**.

72 G. J. Stewart, B. S. Nelson, W. J. F. Acton, A. R. Vaughan, N. J. Farren, J. R. Hopkins, M. W. Ward, S. J. Swift, R. Arya, A. Mondal, R. Jangirh, S. Ahlawat, L. Yadav, S. K. Sharma, S. S. M. Yunus, C. N. Hewitt, E. Nemitz, N. Mullinger, R. Gadi, L. K. Sahu, N. Tripathi, A. R. Rickard, J. D. Lee, T. K. Mandal and J. F. Hamilton,

© 2026 The Author(s). Published by the Royal Society of Chemistry

Environ. Sci.: Atmos., 2026, **6**, 61–75 | **73**

Emissions of Intermediate-Volatility and Semi-Volatile Organic Compounds from Domestic Fuels Used in Delhi, India, *Atmos. Chem. Phys.*, 2021, **21**(4), 2407–2426, DOI: **10.5194/acp-21-2407-2021**.

73 M. A. Santoso, E. G. Christensen, J. Yang and G. Rein, Review of the Transition From Smouldering to Flaming Combustion in Wildfires, *Front. Mech. Eng.*, 2019, **5**(49), DOI: **10.3389/fmech.2019.00049**.

74 M. N. Romanias, M. M. Coggon, F. Al Ali, J. B. Burkholder, P. Dagaut, Z. Decker, C. Warneke, C. E. Stockwell, J. M. Roberts, A. Tomas, N. Houzel, C. Coeur and S. S. Brown, Emissions and Atmospheric Chemistry of Furanoids from Biomass Burning: Insights from Laboratory to Atmospheric Observations, *ACS Earth Space Chem.*, 2024, **8**(5), 857–899, DOI: **10.1021/acsearthspacechem.3c00226**.

75 L. T. Fleming, P. Lin, J. M. Roberts, V. Selimovic, R. Yokelson, J. Laskin, A. Laskin and S. A. Nizkorodov, Molecular Composition and Photochemical Lifetimes of Brown Carbon Chromophores in Biomass Burning Organic Aerosol, *Atmos. Chem. Phys.*, 2020, **20**(2), 1105–1129, DOI: **10.5194/acp-20-1105-2020**.

76 C. D. Zangmeister, R. You, E. M. Lunny, A. E. Jacobson, M. Okumura, M. R. Zachariah and J. G. Radney, Measured *In Situ* Mass Absorption Spectra for Nine Forms of Highly-Absorbing Carbonaceous Aerosol, *Carbon*, 2018, **136**, 85–93, DOI: **10.1016/j.carbon.2018.04.057**.

77 D. T. L. Alexander, P. A. Crozier and J. R. Anderson, Brown Carbon Spheres in East Asian Outflow and Their Optical Properties, *Science*, 2008, **321**(5890), 833–836, DOI: **10.1126/science.1155296**.

78 E. Dalluge, Bio-Mass for Biomass: Biological Mass Spectrometry Techniques for Biomass Fast Pyrolysis Oils, *Doctor of Philosophy*, Iowa State University, Digital Repository, Ames, 2013, **https://dr.lib.iastate.edu/handle/20.500.12876/27795**.

79 E. A. Smith and Y. J. Lee, Petroleomic Analysis of Bio-Oils from the Fast Pyrolysis of Biomass: Laser Desorption Ionization-Linear Ion Trap-Orbitrap Mass Spectrometry Approach, *Energy Fuels*, 2010, **24**(9), 5190–5198, DOI: **10.1021/ef100629a**.

80 D. P. Cole, High Resolution Mass Spectrometry for Molecular Characterization of Pyrolysis Products and Kinetics, *Doctor of Philosophy*, Iowa State University, Digital Repository, Ames, 2015, DOI: **10.31274/etd-180810-3894**.

81 S. Mathai, D. Veghte, L. Kovarik, C. Mazzoleni, K.-P. Tseng, S. Bucci, T. Capek, Z. Cheng, A. Marinoni and S. China, Optical Properties of Individual Tar Balls in the Free Troposphere, *Environ. Sci. Technol.*, 2023, **57**(44), 16834–16842, DOI: **10.1021/acs.est.3c03498**.

82 K. Adachi, A. J. Sedlacek, L. Kleinman, S. R. Springston, J. Wang, D. Chand, J. M. Hubbe, J. E. Shilling, T. B. Onasch, T. Kinase, K. Sakata, Y. Takahashi and P. R. Buseck, Spherical Tarball Particles Form through Rapid Chemical and Physical Changes of Organic Matter in Biomass-Burning Smoke, *Proc. Natl. Acad. Sci. U. S. A.*, 2019, **116**(39), 19336–19341, DOI: **10.1073/pnas.1900129116**.

83 V. P. Kanawade and T. Jokinen, Atmospheric Amines Are a Crucial yet Missing Link in Earth's Climate *via* Airborne Aerosol Production, *Commun. Earth Environ.*, 2025, **6**(1), 98, DOI: **10.1038/s43247-025-02063-0**.

84 X. Ge, A. S. Wexler and S. L. Clegg, Atmospheric Amines – Part I. A Review, *Atmos. Environ.*, 2011, **45**(3), 524–546, DOI: **10.1016/j.atmosenv.2010.10.012**.

85 A. B. Dalton, L. M. Wingen and S. A. Nizkorodov, Isomeric Identification of the Nitroindole Chromophore in Indole + NO₃ Organic Aerosol, *ACS Phys. Chem. Au*, 2024, **4**(5), 568–574, DOI: **10.1021/acsphyschemau.4c00044**.

86 V. J. Baboomian, Q. He, J. Montoya-Aguilera, N. Ali, L. T. Fleming, P. Lin, A. Laskin, J. Laskin, Y. Rudich and S. A. Nizkorodov, Light Absorption and Scattering Properties of Indole Secondary Organic Aerosol Prepared under Various Oxidant and Relative Humidity Conditions, *Aerosol Sci. Technol.*, 2023, **57**(6), 532–545, DOI: **10.1080/02786826.2023.2193235**.

87 D. Lee and A. S. Wexler, Atmospheric Amines – Part III: Photochemistry and Toxicity, *Atmos. Environ.*, 2013, **71**, 95–103, DOI: **10.1016/j.atmosenv.2013.01.058**.

88 B. J. Finlayson-Pitts, Introductory Lecture: Atmospheric Chemistry in the Anthropocene, *Faraday Discuss.*, 2017, **200**, 11–58, DOI: **10.1039/C7FD00161D**.

89 F. Jiang, K. Siemens, C. Linke, Y. Li, Y. Gong, T. Leisner, A. Laskin and H. Saathoff, Molecular Analysis of Secondary Organic Aerosol and Brown Carbon from the Oxidation of Indole, *Atmos. Chem. Phys.*, 2024, **24**(4), 2639–2649, DOI: **10.5194/acp-24-2639-2024**.

90 R. Mayorga, K. Chen, N. Raeofy, M. Woods, M. Lum, Z. Zhao, W. Zhang, R. Bahreini, Y.-H. Lin and H. Zhang, Chemical Structure Regulates the Formation of Secondary Organic Aerosol and Brown Carbon in Nitrate Radical Oxidation of Pyrroles and Methylpyrroles, *Environ. Sci. Technol.*, 2022, **56**(12), 7761–7770, DOI: **10.1021/acs.est.2c02345**.

91 Z. C. J. Decker, K. J. Zarzana, M. Coggon, K.-E. Min, I. Pollack, T. B. Ryerson, J. Peischl, P. Edwards, W. P. Dubé, M. Z. Markovic, J. M. Roberts, P. R. Veres, M. Graus, C. Warneke, J. De Gouw, L. E. Hatch, K. C. Barsanti and S. S. Brown, Nighttime Chemical Transformation in Biomass Burning Plumes: A Box Model Analysis Initialized with Aircraft Observations, *Environ. Sci. Technol.*, 2019, **53**(5), 2529–2538, DOI: **10.1021/acs.est.8b05359**.

92 M. A. J. Harrison, S. Barra, D. Borghesi, D. Vione, C. Arsene and R. Iulian Olariu, Nitrated Phenols in the Atmosphere: A Review, *Atmos. Environ.*, 2005, **39**(2), 231–248, DOI: **10.1016/j.atmosenv.2004.09.044**.

93 N. L. Ng, S. S. Brown, A. T. Archibald, E. Atlas, R. C. Cohen, J. N. Crowley, D. A. Day, N. M. Donahue, J. L. Fry, H. Fuchs, R. J. Griffin, M. I. Guzman, H. Herrmann, A. Hodzic, Y. Iinuma, J. L. Jimenez, A. Kiendler-Scharr, B. H. Lee, D. J. Luecken, J. Mao, R. McLaren, A. Mutzel, H. D. Osthoff, B. Ouyang, B. Picquet-Varrault, U. Platt,

H. O. T. Pye, Y. Rudich, R. H. Schwantes, M. Shiraiwa, J. Stutz, J. A. Thornton, A. Tilgner, B. J. Williams and R. A. Zaveri, Nitrate Radicals and Biogenic Volatile Organic Compounds: Oxidation, Mechanisms, and Organic Aerosol, *Atmos. Chem. Phys.*, 2017, **17**(3), 2103–2162, DOI: **10.5194/acp-17-2103-2017**.

94 M. Kulmala, J. Kontkanen, H. Junninen, K. Lehtipalo, H. E. Manninen, T. Nieminen, T. Petäjä, M. Sipilä, S. Schobesberger, P. Rantala, A. Franchin, T. Jokinen, E. Järvinen, M. Äijälä, J. Kangasluoma, J. Hakala, P. P. Aalto, P. Paasonen, J. Mikkilä, J. Vanhanen, J. Aalto, H. Hakola, U. Makkonen, T. Ruuskanen, R. L. Mauldin, J. Duplissy, H. Vehkamäki, J. Bäck, A. Kortelainen, I. Riipinen, T. Kurtén, M. V. Johnston, J. N. Smith, M. Ehn, T. F. Mentel, K. E. J. Lehtinen, A. Laaksonen, V.-M. Kerminen and D. R. Worsnop, Direct Observations of Atmospheric Aerosol Nucleation, *Science*, 2013, **339**(6122), 943–946, DOI: **10.1126/science.1227385**.

95 L. Yao, O. Garmash, F. Bianchi, J. Zheng, C. Yan, J. Kontkanen, H. Junninen, S. B. Mazon, M. Ehn, P. Paasonen, M. Sipilä, M. Wang, X. Wang, S. Xiao, H. Chen, Y. Lu, B. Zhang, D. Wang, Q. Fu, F. Geng, L. Li, H. Wang, L. Qiao, X. Yang, J. Chen, V.-M. Kerminen, T. Petäjä, D. R. Worsnop, M. Kulmala and L. Wang, Atmospheric New Particle Formation from Sulfuric Acid and Amines in a Chinese Megacity, *Science*, 2018, **361**(6399), 278–281, DOI: **10.1126/science.aao4839**.

96 C. Qiu and R. Zhang, Physiochemical Properties of Alkylaminium Sulfates: Hygroscopicity, Thermostability, and Density, *Environ. Sci. Technol.*, 2012, **46**(8), 4474–4480, DOI: **10.1021/es3004377**.

97 E. Dinar, T. Anttila and Y. Rudich, CCN Activity and Hygroscopic Growth of Organic Aerosols Following Reactive Uptake of Ammonia, *Environ. Sci. Technol.*, 2008, **42**(3), 793–799, DOI: **10.1021/es071874p**.

98 J. N. Smith, K. C. Barsanti, H. R. Friedli, M. Ehn, M. Kulmala, D. R. Collins, J. H. Scheckman, B. J. Williams and P. H. McMurry, Observations of Aminium Salts in Atmospheric Nanoparticles and Possible Climatic Implications, *Proc. Natl. Acad. Sci. U. S. A.*, 2010, **107**(15), 6634–6639, DOI: **10.1073/pnas.0912127107**.

99 X. Hu, Z. Guo, W. Sun, X. Lian, Y. Fu, H. Meng, Y. Zhu, G. Zhang, X. Wang, L. Xue, X. Bi, X. Wang and P. Peng, Atmospheric Processing of Particulate Imidazole Compounds Driven by Photochemistry, *Environ. Sci. Technol. Lett.*, 2022, **9**(4), 265–271, DOI: **10.1021/acs.estlett.2c00029**.

100 M. Teich, D. Van Pinxteren, S. Kecorius, Z. Wang and H. Herrmann, First Quantification of Imidazoles in Ambient Aerosol Particles: Potential Photosensitizers, Brown Carbon Constituents, and Hazardous Components, *Environ. Sci. Technol.*, 2016, **50**(3), 1166–1173, DOI: **10.1021/acs.est.5b05474**.

101 H. J. Lee, P. K. Aiona, A. Laskin, J. Laskin and S. A. Nizkorodov, Effect of Solar Radiation on the Optical Properties and Molecular Composition of Laboratory Proxies of Atmospheric Brown Carbon, *Environ. Sci. Technol.*, 2014, **48**(17), 10217–10226, DOI: **10.1021/es502515r**.

102 P. K. Aiona, H. J. Lee, R. Leslie, P. Lin, A. Laskin, J. Laskin and S. A. Nizkorodov, Photochemistry of Products of the Aqueous Reaction of Methylglyoxal with Ammonium Sulfate, *ACS Earth Space Chem.*, 2017, **1**(8), 522–532, DOI: **10.1021/acsearthspacechem.7b00075**.

© 2026 The Author(s). Published by the Royal Society of Chemistry

Environ. Sci.: Atmos., 2026, **6**, 61–75 | **75**